Article ID: 1005-9784(2005)04-0494-05

Quantitative study of atmospheric effects in spaceborne InSAR measurements①

LI Zhi-wei(李志伟)[1,2], DING Xiao-li(丁晓利)[2], ZHU Jian-jun(朱建军)[2], ZOU Zheng-rong(邹峥嵘)[1]
(1. School of Info-physics and Geomatics Engineering, Central South University, Changsha 410083, China;
2. Department of Land Surveying and Geo-informatics, Hong Kong Polytechnic University, Kowloon, Hong Kong, China)

Abstract: Atmospheric effects on interferometric synthetic aperture radar(InSAR) measurements are quantitatively studied based on a tandem pair of SAR data and a month long continuous GPS tracking data obtained at six stations. Differential atmospheric signals extracted from the SAR data for two selected areas show apparent power law characteristics. The RMS values of the signals are 2.04 and 3.66 rad respectively for the two areas. These differential delays can potentially cause in the two areas peak to peak deformation errors of 3.64 and 6.52 cm, respectively, at the 95% confidence level and Gaussian distribution. The respective potential peak to peak DEM errors are 123 and 221 m. The GPS tropospheric total zenith delays estimate indicates that a peak to peak error of about 7.8 cm can potentially be caused in a SAR interferogram with only 1 d interval at the 95% confidence level. The error increases to about 9.6 cm for 10 d interval. The potential peak to peak DEM and deformation errors estimated from GPS total zenith delay measurements are however quite similar to those estimated from InSAR data. This provides us with a useful tool to pre-estimate the potential atmospheric effects in a SAR interferogram before we order the SAR images. Nevertheless, the results reveal that even in a small area the atmospheric delays can obscure centimetre level ground displacements and introduce a few hundred meters of errors to derived DEM.

Key words: atmospheric effect; InSAR; GPS; power law; total zenith delay
CLC number: P237 **Document code**: A

1 INTRODUCTION

Interferometric synthetic aperture radar (InSAR) has been widely applied in recent years. Its all-weather, day and night imaging capabilities, and unprecedented spatial coverage and resolution make it a unique technology for topographic mapping and ground displacement monitoring. InSAR has however some weaknesses. One of the most intractable problems is the atmospheric effect, especially the atmospheric water vapor, on repeat-pass SAR data[1-7]. Due to the highly variable nature of the atmosphere, it is difficult to construct an accurate model and correct the atmospheric effects, especially in humid regions[5].

This paper aims to assess the atmospheric effects on InSAR measurements in humid regions using both InSAR and GPS data. The principles of repeat-pass InSAR and atmospheric effect on InSAR will be briefly outlined first. The processing of the SAR and GPS data will then be introduced and the results are finally analyzed.

2 REPEAT-PASS INSAR

The phase measurements of repeat-pass InSAR system can be written as (Fig. 1):

$$\psi_1=\frac{4\pi}{\lambda}\rho_1,\quad \psi_2=\frac{4\pi}{\lambda}\rho_2 \tag{1}$$

where ρ_1 and ρ_2 are the slant ranges of the first and second acquisitions, respectively, and λ is the radar wavelength. The interferometric phase φ is then

$$\varphi=\psi_1-\psi_2=\frac{4\pi}{\lambda}(\rho_1-\rho_2) \tag{2}$$

Under the far field approximation,

$$\varphi=\psi_1-\psi_2\approx\frac{4\pi}{\lambda}B^{\parallel}=\frac{4\pi}{\lambda}B\sin(\theta_0+\delta\theta-\alpha) \tag{3}$$

where α is the orientation angle of the baseline and θ is the look angle.

Assuming a surface without topographic relief as shown in Fig. 1, the interferometric phase becomes:

$$\varphi_0=\frac{4\pi}{\lambda}B\sin(\theta_0-\alpha) \tag{4}$$

Combining Eqns. (3) and (4), the "flattened" phase is:

$$\varphi_{\text{flat}}=\varphi-\varphi_0\approx\frac{4\pi}{\lambda}B\cos(\theta_0-\alpha)\,\delta\theta\approx\frac{4\pi}{\lambda}B^{\perp}\delta\theta \tag{5}$$

① **Foundation item**: Project (40404001) supported by the National Natural Science Foundation of China; project (WKL(03)0104) supported by the State Key Laboratory for Information Engineering of Surveying, Mapping and Remote Sensing
Received date: 2004-12-07; **Accepted date**: 2005-02-01
Correspondence: LI Zhi-wei, PhD, lecturer; E-mail: zwli@mail.csu.edu.cn

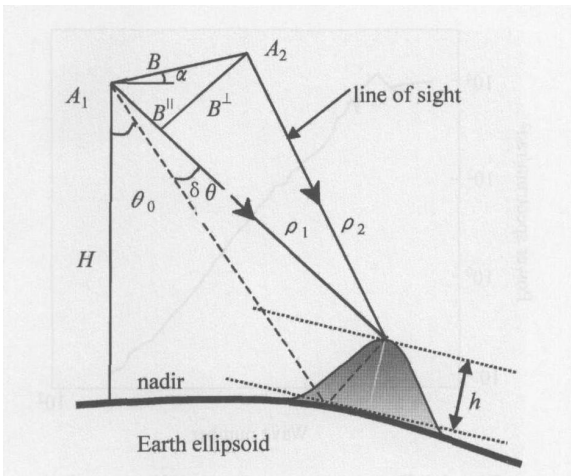

Fig. 1 Interferometric geometry

Thus the topographic height can be expressed as

$$h \approx \rho \delta\theta \cdot \sin\theta_0 = \frac{\lambda}{4\pi B^{\perp}} \rho \sin\theta_0 \varphi_{\text{flat}} \qquad (6)$$

If there exists a ground deformation Δr along the radar line of sight (LOS) direction between the two acquisitions, it will also manifest itself in the interferometric phase:

$$\varphi - \varphi_0 \approx \frac{4\pi}{\lambda} \frac{B^{\perp}}{\rho \sin\theta_0} h + \frac{4\pi}{\lambda} \Delta r \qquad (7)$$

3 ATMOSPHERIC EFFECTS ON REPEAT PASS INSAR

Two types of errors may potentially be introduced when microwave propagates through the troposphere, the ray bending and the propagation delays. The latter dominates in case of InSAR measurements. Taking into consideration the propagation delay errors in InSAR, the phase measurements become:

$$\psi_1 = \frac{4\pi}{\lambda}(\rho_1 + \Delta\rho_1), \quad \psi_2 = \frac{4\pi}{\lambda}(\rho_2 + \Delta\rho_2) \qquad (8)$$

The interferometric phase is then

$$\varphi = \psi_1 - \psi_2 = \frac{4\pi}{\lambda}(\rho_1 - \rho_2) + \frac{4\pi}{\lambda}(\Delta\rho_1 - \Delta\rho_2) \qquad (9)$$

where $\frac{4\pi}{\lambda}(\Delta\rho_1 - \Delta\rho_2)$ is the contributions from atmosphere, which can be cancelled out if the atmospheric profile remains the same between the two acquisitions. Besides, the atmospheric effects will also be cancelled out if the atmospheric induced interferometric phase shifts are the same for all the resolution cells in an area of interest[3]. The two conditions however rarely occur. First, the troposphere, especially the tropospheric water vapor, varies significantly over a periods of a few hours or even shorter. It is therefore difficult to have the same atmospheric profiles even over the shortest revisit interval of 1 d(for ERS 1/2). Second, it is also highly unlike for the relative tropospheric delays to be constant for all the resolution cells due to local turbulent mixing of troposphere. The atmospheric signatures are easily mis interpreted as the topographic or ground deformation signals or noise.

An SAR interferogram generated by complex conjugate multiplication of two SAR images is a superposition of information on topography height, surface deformations, differential atmospheric delays between the acquisitions and the noise[4]. If there is no surface deformation between the two image acquisitions or if the deformation is known, the atmospheric signatures can be extracted from an interferogram by eliminating the contribution of the topography and suppressing interferometric noise.

An ESA ERS Tandem pair acquired on March 18 and 19, 1996 over southern China is used for this purpose. The perpendicular baseline of the SAR pair is 100 m. As the two images have only an interval of 1 d, it can be safely assumed that there is no surface deformation between the SAR acquisitions. Since satellite orbit errors generate in an interferogram long wavelength phase shifts similar to the long wavelength atmospheric disturbances[7], careful baseline refinement is necessary in the interferometric processing. Besides, the phase ramp that is caused by residual flat earth phase and residue orbit errors are removed with linear model. Fig. 2 shows one of the amplitude images, where rectangles A and B, a flat and a hilly areas respectively, are chosen for further study. The two areas are about 6 km × 11 km and 5 km × 10 km respectively in size. Since even the small scales traveling ionospheric disturbances have a wavelength of tens of kilometers, the ionospheric effects on these two relatively small areas can be considered neglectable[3].

For area A, since the perpendicular baseline is not too large and the majority of the surface varies within 5 – 10 m except for a small ridge in the northwest part, the variations of the interferometric phase are largely due to radar signal path delays caused by the atmosphere. For area B, a DEM created from the digital map was used to remove the topographic component from the interferogram. Fig. 3 shows the unwrapped interferometric phases, i. e., differential atmospheric phases, in the two areas. The mean differential atmospheric delays in each of the areas are then calculated and removed from their unwrapped interferogram. A 2D Fast Fourier Transform (FFT) is performed next for each of the areas and the results are squared to obtain the power spectra. The 1D rotationally averaged power spectra are given in Figs. 4 and 5, respectively.

The power spectra of the differential atmos

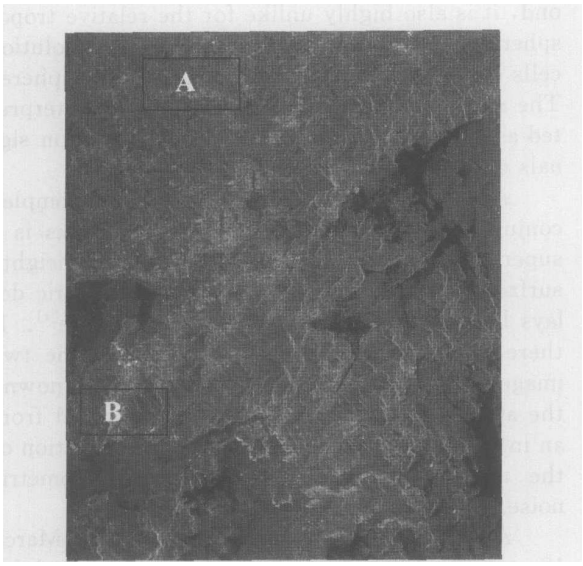

Fig. 2 SAR amplitude image
(A and B are flat and hilly areas, respectively)

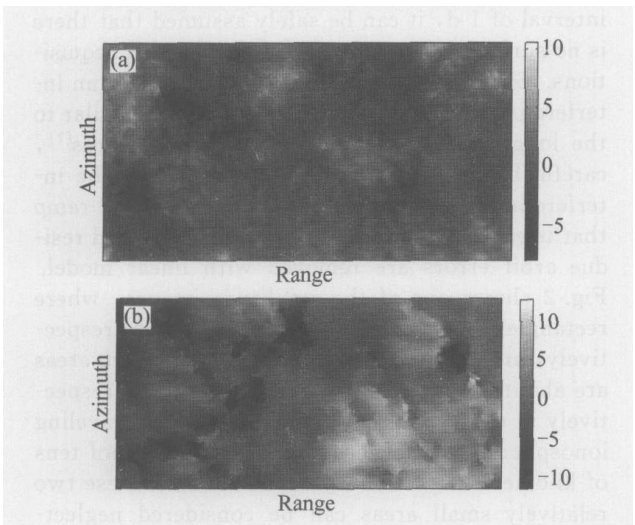

Fig. 3 Unwrapped interferometric phases for areas A(a) and B(b) with topographic phase removed

pheric delays in both of the areas on the whole follow the power law, which is commonly associated with the Kolmogorov turbulence[8]. The results are in good agreement with those presented by Hanssen[4, 9]. The dashed lines in the figures follow a slope of −8/3. The power law index varies with the scales slightly, which is consistent with the turbulence behavior of such phenomena as integrated water vapor, and the wet delays in radio ranging[10]. This power law spectra characteristic is very useful in the handling of atmospheric effects in InSAR. For example. Ferretti et al[11] took advantage of the particular spectra (or frequency) characteristics to estimate the atmospheric effects and the noise powers separately for each interferogram and based on the results developed a method

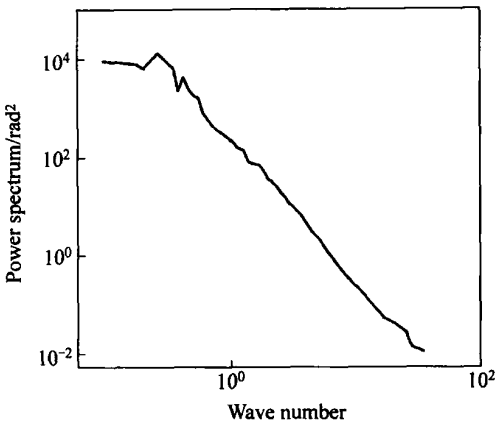

Fig. 4 Power spectrum of differential atmospheric delays for area A

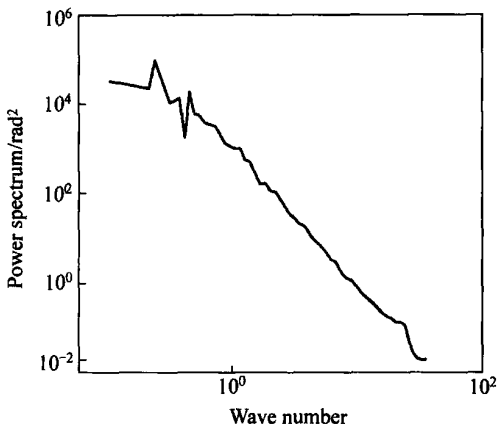

Fig. 5 Power spectrum of differential atmospheric delays for area B

to combine the resulted SAR DEMs by means of a weighted average in wavelet domain instead of the simple average[11-14]; Ferretti et al[12] utilized the frequency characteristic to design filters to separate atmospheric effects from nonlinear subsidence; LI et al[6, 15] incorporated the power law nature in designing algorithms to integrate CGPS and meteorological data for atmospheric effects mitigation.

Though in both of the areas the power spectra follow the power law, the absolute power of differential atmospheric delay in area B is larger than that of area A. This more or less indicates the severeness of atmospheric effects in these two areas. As noted by Hanssen[4], in flat area, only the turbulent mixing process of troposphere will affect InSAR measurements, whilst in mountainous area both turbulent mixing and vertical stratification exert effects.

The RMS errors of the differential atmospheric delays for the two areas are 2.04 and 3.66 radians, respectively. On the assumption of Gaussian distribution, the differential atmospheric delays might vary from −4.08 to 4.08 radians in area A,

and from -7.32 to 7.32 radians in area B at the 95% confidence level. This constitutes in these two areas the peak-to-peak variabilities of 8.16 and 14.64 radians, respectively. The potential peak-to-peak DEM (assuming a 100 m perpendicular baseline) and deformation errors thus introduced are listed in Table 1. This level of tropospheric variations can make cm-level ground displacements unobservable and introduce hundreds of meters error in DEM.

Table 1 Potential errors in InSAR measurements (estimated from InSAR data)

	Area A	Area B
Peak to peak deformation error/cm	3.64	6.52
Peak to peak DEM error/m	123	221

4 COMPARISON WITH GPS TRACKING DATA

Tropospheric total zenith delays (TZD) at Continuous GPS (CGPS) stations can be estimated along with other geodetic parameters. The accuracy of TZDs estimated from GPS measurements is generally better than 10 mm, and may reach 5 mm[10]. Since the troposphere is a non-dispersive medium, we can use the TZDs estimated from CGPS to assess the atmospheric effects on InSAR after they are converted to the radar LOS direction.

There are currently six CGPS stations in the area covered by SAR interferogram. The stations all started operations in 2000 or earlier. In this study, we applied the GPS data for one month (March 1st to 31st, 2001) at the six stations and five IGS stations, i.e., LHAS, SHAO, TAIW, WHHN and XIAN, to resolve the hourly TZDs of the stations. The IGS precise orbits were used in the solutions and the cut-off angle chosen for the GPS data was 20°. SHAO was fixed and the other stations were tightly constrained. The variations of the TZDs were treated as first-order Gauss-Markov processes. Due to some data recording problems, the hourly TZDs on March 26th, 27th 2001 could not be used for all the stations, neither could those on March 20th, 21st and 22nd 2001 for Siulangshui and on March 6th 2001 for Kauyichau. The estimated TZDs for the six stations are shown in Fig. 6. The discontinuities in the plots are due to data gaps.

Since it is the differential atmospheric delays that affect the InSAR measurements, we will look more closely at the differentiated TZDs. The differentiated TZDs at each of the GPS stations for one day and ten-day intervals are calculated firstly, then hourly standard deviation (SD) of the differentiated TZDs at six GPS stations is calculated. A summary of the SDs is given in Table 2.

For the one-day interval, the largest, smallest and mean SDs of the differenced TZDs are 2.31, 0.16 and 0.90 cm, respectively. The 0.90 cm mean SD is translated into a 95% confidence interval of -1.8 cm to 1.8 cm with the assumption of Gaussian distribution. The corresponding mean SD for the ten days interval is 1.09 cm and its 95% confidence interval is -2.2 cm to 2.2 cm. When assuming the looking angle to be 23° (the looking angle of the mid-scene of the ERS-1/2 images), the vari-

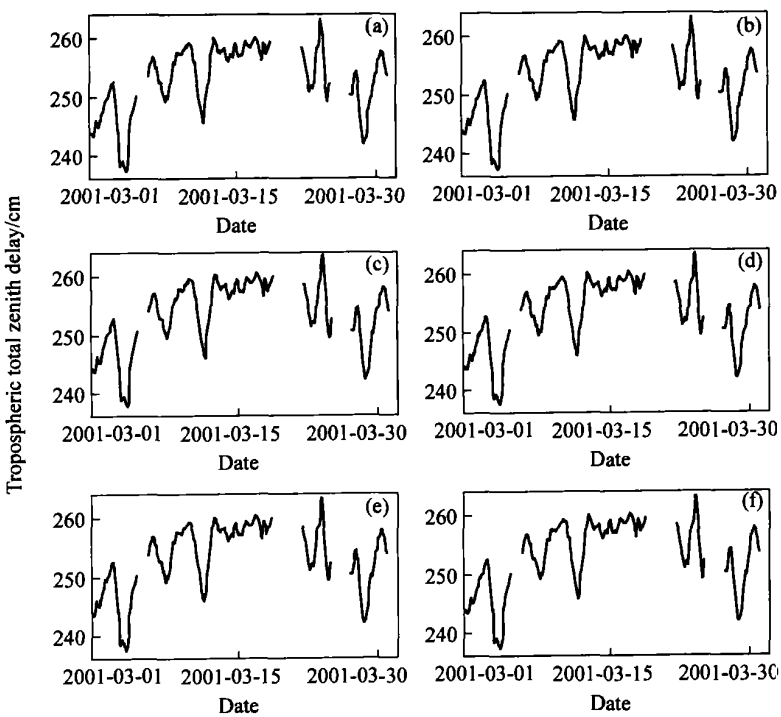

Fig. 6 Hourly tropospheric TZD values at six GPS tracking stations
(a)—Fanling; (b)—Kantin; (c)—Kauyichau; (d)—Lam tei, (e)—Siulangshui; (f)—Shatin

Table 2 Standard deviations of the differenced TZDs

Interval/d	Maximum value/cm	Minimum value/cm	Mean value/cm
1	2.31	0.16	0.90
10	2.38	0.21	1.09

ations are translated into 7.8 cm and 9.6 cm of round trip radar signal delays. The potential peak-to-peak DEM and deformation errors introduced are listed in Table 3. This level of tropospheric variations can also make cm level ground displacements unobservable and introduce hundreds of meters error in DEM for a perpendicular baseline of 100 m.

Table 3 Potential errors in InSAR measurements (estimated from GPS data)

	1 d	10 d
Peak to peak deformation error/cm	3.9	4.8
Peak to peak DEM error/m	132	163

From Table 3, it can be seen that the magnitudes of the potential peak-to-peak DEM and deformation errors for 1 d interval are quite similar to those estimated from InSAR data (see Table 1). This demonstrates that GPS TZDs can be used to quantitatively assess the degree of atmospheric effect on InSAR prior to InSAR processing. This can be severed as a caution for InSAR image planning.

5 CONCLUSIONS

Atmospheric effects on InSAR measurements have been quantitatively studied for southern China region based on an SAR tandem image pair and a month-long GPS data obtained at six stations. The differential atmospheric delays determined from the SAR interferogram for two selected areas clearly follow the power law, consistent with results obtained by other researchers. The RMS values of the differential atmospheric delays for the two areas are 2.04 and 3.66 rad, respectively. On the assumption of Gaussian distribution and at 95% confidence level, they can potentially cause in the two areas peak-to-peak deformation errors of 3.64 and 6.52 cm, respectively. The respective potential peak-to-peak DEM errors in these two areas are 123 and 221 m on the further assumption of 100 m perpendicular baseline. The atmospheric effects are more serious in mountainous regions than in flat region.

The tropospheric TZDs estimated from GPS measurements have shown significant temporal and spatial variations. They can potentially cause a peak-to-peak error of about 7.8 cm to a SAR interferogram at the 95% confidence level for the one day interval. The error increases to about 9.6 cm for 10 d interval. The magnitude of the potential peak-to-peak errors thus estimated are quite similar to those estimated from InSAR data. This demonstrates that GPS TZDs can be used to quantitatively assess the degree of atmospheric effect on InSAR. Nevertheless, even in a small experiment area in humid region the atmospheric delays can obscure centimetre level ground displacements and introduce a few hundred meters of errors to the measured terrain heights.

REFERENCES

[1] Goldstein R M. Atmospheric limitations to repeat track radar interferometry[J]. Geophysical Research Letters, 1995, 22(18): 2517-2520.

[2] Zebker H A, Rosen P A, Hensley S. Atmospheric effects in interferometric synthetic aperture radar surface deformation and topographic maps[J]. Journal of Geophysical Research, 1997, 102(B4): 7547-7563.

[3] Hanssen R F. Radar Interferometry: Data Interpretation and Error Analysis[M]. Dordrecht: Kluwer Academic Press, 2001.

[4] Hanssen R F, Wechwerth T M, Zebker H A, et al. High-resolution water vapor mapping from interferometric radar measurements[J]. Science, 1999, 283: 1297-1299.

[5] Li Z W, Ding X L, Liu G X, et al. Atmospheric effects on InSAR measurements—a review[J]. Geomatics Research Australasia, 2003, 79: 43-58.

[6] Li Z W, Ding X L, Liu G X. Modeling atmospheric effects on InSAR with meteorological and continuous GPS observations: algorithms and some test results[J]. Journal of Atmospheric and Solar Terrestrial Physics, 2004, 66: 907-917.

[7] Tarayre H, Massonnet D. Atmospheric propagation heterogeneities revealed by ERS 1[J]. Geophysical Research Letters, 1996, 23(9): 989-992.

[8] Tatarski V I. Wave Propagation in a Turbulent Medium[M]. New York: McGraw Hill, 1961.

[9] Hanssen R F. Atmospheric Heterogeneities in ERS Tandem SAR Interferometry[M]. Felft: Delft University Press, 1998.

[10] Ruf C S, Beus S E. Retrieval of tropospheric water vapor scale height from horizontal turbulence structure[J]. IEEE Transactions on Geoscience and Remote Sensing, 1997, 35(2): 203-211.

[11] Ferretti A, Prati C, Rocca F. Multibaseline InSAR DEM reconstruction: the wavelet approach[J]. IEEE Transactions on Geoscience and Remote Sensing, 1999, 37(2): 705-715.

[12] Ferretti A, Prati C, Rocca F. Nonlinear subsidence rate estimation using permanent scatters in differential SAR interferometry[J]. IEEE Transactions on Geoscience and Remote Sensing, 2000, 38(5): 2202-2212.

[13] Liu Y X. Remote Sensing of Water Vapor Content Using GPS Data in Hong Kong Region[D]. Hong Kong: Hong Kong Polytechnic University, 1999.

[14] Rosen P A, Hensley S, Zebker H A, et al. Surface deformation and coherence measurements of kilauea volcano, hawaii, from SIR C radar interferometry[J]. Journal of Geophysical Research, 1996, 101(E10): 23109-23125.

[15] LI Zhi-wei. Modelling Atmospheric Effects in Repeat-pass InSAR Measurements[D]. Hong Kong: Hong Kong Polytechnic University, 2005.

(**Edited by CHEN Can-hua**)